Kinetic study of time-dependent fixation of U^{VI} on biochar.

A. Ashry [a,b], E.H. Bailey [a*], S.R.N. Chenery [c] and S.D. Young [a]

a. Division of Agricultural and Environmental Sciences, School of Biosciences, University of Nottingham, Sutton Bonington, Leicestershire LE12 5RD, UK.
b. Radiation Protection Department, Nuclear Research Centre, Egyptian Atomic Energy Authority, Cairo, Egypt.
c. British Geological Survey, Nicker Hill, Keyworth, Nottingham NG12 5GG, UK.

*Corresponding author: liz.bailey@nottingham.ac.uk, Tel:+44(0)1159516255

Abstract

Biochar, a by-product from the production of biofuel and syngas by gasification, was tested as a material for adsorption and fixation of U^{VI} from aqueous solutions. A batch experiment was conducted to study the factors that influence the adsorption and time-dependent fixation on biochar at 20°C, including pH, initial concentration of U^{VI} and contact time. Uranium (U^{VI}) adsorption was highly dependent on pH but adsorption on biochar was high over a wide range of pH values, from 4.5 to 9.0, and adsorption strength was time-dependent over several days. The experimental data for pH > 7 were most effectively modelled using a Freundlich adsorption isotherm coupled to a reversible first order kinetic equation to describe the time-dependent fixation of U^{VI} within the biochar structure. Desorption experiments showed that U^{VI} was only sparingly desorbable from the biochar with time and isotopic dilution with $^{233}U^{VI}$ confirmed the low, or time-dependent, lability of adsorbed $^{238}U^{VI}$. Below pH 7 the adsorption isotherm trend suggested precipitation, rather than true adsorption, may occur. However, across *all* pH values (4.5–9) measured saturation indices suggested precipitation was possible: autunite below pH 6.5 and either swartzite, liebigite or bayleyite above pH 6.5.

Keywords: biochar, uranium, adsorption, pH, isotherm and kinetics

1 Introduction

Increasing demand for energy has persuaded many countries to look for alternative and renewable sources such as biofuel and syngas [1]. Their production by gasification, pyrolysis or hydrothermal carbonization (HTC) of plant or animal biomass (e.g. wood, manure, leaves or bone) in an oxygen deficient environment [2] generates large quantities of carbonaceous by-products known collectively as 'biochar' [3]. The composition and properties of biochar depend upon the production method and source material being combusted. This results in variation in physical and chemical properties such as pH, ash content, surface area and chemistry [4]. Material produced from gasification and/or pyrolysis has a higher ash content than biochar produced via HTC which is richer in carbon [3]. Comparison of the characteristics of biochars produced from the same pinewood source material by HTC at 300^{o}C or pyrolysis at 700^{o}C for copper adsorption from aqueous solution [5] found that HTC-biochar had more active adsorption sites and stable carbon-oxygen complexes on its surface with a 95% increase in oxygen-containing groups compared to the source material. By contrast, there was a 56% decrease in oxygen-containing groups in biochar produced by pyrolysis. BET surface area measurements showed that the biochar produced by HTC had a lower surface area (21 $m^2\ g^{-1}$) compared to the biochar produced via pyrolysis (29 $m^2\ g^{-1}$), but had a greater capacity to adsorb copper.

Biochar was first used as a soil amendment at Terra Preta de Indio, in the Amazon region by ancient Amerindian populations [2]. In soils it has been shown to improve biological nitrogen fixation, increase nutrient retention and immobilize phytotoxic heavy metals [6]. Other applications claimed include waste management and mitigation of climate changes [2]. Biochar has recently attracted attention as a potential adsorbent in water purification as it contains oxygen-substituted functional groups (e.g. carboxylic, lactone and phenolic groups) embedded within a highly porous structure. As a consequence it has a large capacity for adsorption of heavy metals, radionuclides and organic pollutants, particularly from aqueous media [5, 7, 8]. Many studies have reported that the time to reach equilibration for heavy metal sorption is <24 h [9-11]. It has also been suggested that the sorption kinetics are not limited by diffusion of metal ions into biochar pores but by surface precipitation with carbonate, phosphate and/or silicate [12]. The kinetics and reversibility of reactions between binder and contaminant are particularly important when considering water purification applications as distinct from a possible role as a soil amendment.

Few studies have examined the capacity of biochar for removal of radioactive materials from aqueous solutions or its potential as a soil amendment for the remediation of radioactively contaminated soil. Biochar produced from HTC of switch grass was investigated as a potential permeable reactor barrier material [3]. The U^{VI} adsorption capacity increased from 2120 mg kg^{-1} at pH 3.0 to ~4000 mg kg^{-1} at pH 5.9 then declined at higher pH. This suggests that U^{VI} adsorption is highly dependent on the U speciation in solution with formation of carbonate complexes at higher pH. Factors affecting U removal and recovery from aqueous solutions by HTC-biochar including pH, initial U^{VI} concentration, contact time, ionic strength and temperature have also been investigated [13]. Maximum uptake capacity was attained at a pH of ~6.0 after 50 minutes equilibration. A pseudo-second order kinetic model best described the adsorption kinetics and a Langmuir adsorption isotherm described the adsorption process at equilibrium. The thermodynamic parameters ΔG^o (298 K^o) ΔH^o and ΔS^o defining the adsorption reaction were reported as -14.4, 36.1 kJ mol^{-1} and 169.7 J mol^{-1} K^{-1}, respectively, indicating that U^{VI} sorption on biochar was endothermic [13]. Regeneration of the biochar was possible by leaching with 0.05 mol L^{-1} HCl solution, possibly suggesting reversible bonding to oxyacid surface groups.

The aim of the current study was to investigate the ability of a phosphate-rich bone-derived biochar to adsorb and fix U^{VI} from solution over a period of 15 days. Most biochars are of plant/wood origin whereas bone biochar, used in this study, has dual characteristics in that it consists of a carbon-based matrix in intimate association with a Ca phosphate mineral phase. The underlying hypothesis was that while oxy-acid functional groups on the biochar (e.g. COOH) provide sites for rapid adsorption of U^{VI} a longer-term fixation mechanism might result from gradual incorporation into the apatite structure with UO_2^{2+} ions replacing Ca^{2+}. The main objectives of this work were to address the questions:

i. Does biochar show time-dependent fixation of U^{VI} or is the adsorption reaction wholly reversible and rapid?
ii. What factors affect the strength of adsorption and fixation of U^{VI} in the biochar and what underlying mechanisms appear to operate?
iii. Is the bone-biochar a suitable material for water purification or better suited to soil remediation?

Batch U adsorption data were fitted to kinetic and diffusion models which assumed rapid reversible adsorption coupled with a slower 'fixation' reaction to explain the time-dependence of the reaction between U^{VI} and the bone-biochar. The effect of solution pH and U loading on the reaction kinetics were investigated. The desorbability of the (adsorbed) U^{VI} was assessed using desorption into a solution matrix in which only the U^{VI} concentration differed from the pre-equilibrated adsorption solution. An attempt was made to use isotopic dilution with $^{233}U^{VI}$ to quantify the 'reactivity' (lability) of the previously adsorbed U^{VI}. The free ion activity products of candidate solid phases were tested for possible surface precipitation of U on biochar. We believe this is the first study to quantify, and model, uranium fixation in a phosphatic biochar through concurrent measurement of (i) adsorption kinetics, (ii) desorbability and (iii) isotopic exchangeability with enriched ^{233}U.

2 Materials and methods

All chemicals and reagents were of trace analysis grade unless otherwise stated. All solutions were prepared using Milli-Q water (~18 MΩ cm, TOC ≤10 µg L^{-1}). Uranium calibration standards and $^{238}U^{VI}$ spike solution were prepared by dilution of a stock ICP-MS standard solution containing 1000 mg L^{-1} U^{VI} dissolved in 2% HNO_3.

Biochar, produced from gasification of cow bone in the absence of oxygen at approximately 850°C, was obtained from Brimac Environmental Services Ltd., Greenock, UK and dried at room temperature for 1 week.

2.1 Instrumentation

2.1.1 Inductively coupled plasma mass spectrometry (ICP-MS)

Elemental analysis was undertaken by quadrupole ICP-MS (iCAP-Q, Thermo Scientific) employing a peltier-cooled spray chamber equipped with concentric quartz glass nebulizer. Internal standards included Rh (20 µg L^{-1}) and Ir (10 µg L^{-1}) in 2% HNO_3. Trace elements were calibrated using Claritas-PPT grade CLMS-2 (Certiprep/Fisher); Major alkali(-earth) cations were calibrated using a bespoke standard (PlasmaCAL, SCP Science, France) and P, B and S calibrations utilized an in-house standard solution (KH_2PO_4, K_2SO_4 and H_3BO_3). Limits of detection (µg L^{-1}) were: Ca (13.8), Mg (0.41), P (3.51), ^{238}U (0.00028), ^{233}U (0.00001). In-sample switching was used to measure B and P in STD mode, Se in H_2-cell mode and all other elements in He-cell mode. Peak dwell times were 10 mS for most elements with 150 scans per sample. Sample processing was undertaken using Qtegra™ Intelligent Scientific Data Solution™ (ISDS) software (Thermo- Fisher Scientific, UK).

2.1.2 Scanning electron microscopy (SEM)

Grains of biochar were mounted on double-sided adhesive carbon tabs fixed to 10 mm diameter aluminium SEM stubs. Images were taken on uncoated samples using an FEI Quanta600 environmental scanning electron microscope (ESEM) equipped with an

Oxford Instruments INCA Energy 450 energy-dispersive X-ray microanalysis (EDXA) system and silicon drift X-ray detector (SDD) capable of operating at high input X-ray count rates (up to ~106 counts per second). The ESEM was operated in low vacuum mode, with an accelerating voltage of 20 kV, beam probe currents of c.0.6 nA and a working distance of ~10 mm [14].

2.1.3 Biochar Elemental Composition

Biochar was acid digested using a mixed HF-HNO_3-$HClO_4$ acid protocol. Biochar samples (c. 0.200 g) in triplicate were weighed into PFA vials and heated on a 48-place Teflon-coated graphite block digester with 4 ml of concentrated HNO_3 for 30 min to digest the organic fraction. A further 2 ml of HNO_3 and 1 ml of $HClO_4$ were then added with heating at 80°C for 8 hr and then at 100°C for a further 2 hr. An aliquot (2.5 ml) of hydrofluoric acid (40% AR) was added and samples were heated to 120°C for 8 hr until dry. Finally, 2.5 ml of HNO_3 and 2.5 ml of Millli-Q water were added and the samples left for one hour at 50°C. Finally, the digestate was made to 50 ml by adding Millli-Q water. Operational blanks were prepared in the same way. Analysis of C%, N% and H% was undertaken in duplicate using a FLASH 2000 CHNS/O Analyzer (Thermo Fisher Scientific). Inorganic C% was determined in triplicate using a Shimadzu TOC-VCS/CP analyzer SSM-5000A.

2.1.4 Dissolved organic and inorganic carbon

Total dissolved carbon (TC) and dissolved organic carbon (DOC) were determined on biochar suspensions in 0.01 M $Ca(NO_3)_2$ using a Shimadzu TOC-VCPH. Samples were acidified with HCl to pH 2-3 to remove inorganic carbon, before the remaining (organic) carbon was detected as CO_2 by non-dispersive infrared detection after heating to 720°C with a platinum-coated alumina catalyst. Inorganic carbon was estimated from the difference between TC and DOC.

2.2 Batch adsorption experiment

Batch sorption experiments of U^{VI} on biochar were undertaken in duplicate. Biochar was pre-equilibrated at room temperature for 10 days with 0.01 M $Ca(NO_3)_2$ as a background electrolyte on an end-over-end vertical rotary shaker after addition of 0.5 M HNO_3 to adjust the pH to a range of values (pH = 4.5, 5, 6, 7, 8 and 9) prior to addition of U^{VI} spikes. The added U^{VI} concentrations (U_{added}) were 0.1, 0.5, 1, 2, 3 and 5 mg L^{-1} in an overall volume of 30 ml. The suspensions (33.3 g L^{-1}) were shaken for 15 days and subsamples collected after contact times (t) of 1, 2, 3, 4, 5, 7 and 15 days. Each suspension was allowed to settle (30 min) before a subsample was filtered (<0.22 μm) and acidified (2% HNO_3) for elemental analysis. A further aliquot was diluted and analysed for DOC and DIC.

The amount of U^{VI} adsorbed (U_{ads}, mg kg^{-1}) was determined from the difference between the added U^{VI} concentration (U_{added}, mg L^{-1}) and measured solution U concentration (U_{soln}, mg L^{-1}) from Eq.(1):

$$U_{ads} = (U_{added} - U_{soln}) * \left(\frac{V}{W}\right) \quad (1)$$

where V is the total volume of suspension (L) and W the weight of biochar (kg).

2.2.1 Reversible first order model (RFO)

A reversible first order kinetic model (RFO) was used to describe the time-dependent adsorption of U^{VI} onto the biochar. Following the initial rapid attainment of a reversible equilibrium, further sorption was considered as a time-dependent, but reversible, reaction:

$$U^{VI} + Bio - S \underset{k_b}{\overset{k_a}{\leftrightarrows}} Bio - S - U^{VI}$$

Where k_a and k_b are reversible first order forward and reverse rate constants, respectively and Bio-S is the active site on the biochar surface.

The first order model equation can be expressed as described in Eq.(2) [15]:

$$[U]_t = [U]_o \left(\frac{k_b + k_a e^{-(k_a+k_b)t}}{k_a+k_b}\right) \quad (2)$$

where $[U]_o$ is the initial concentration of U^{VI} in solution at 'time zero', established instantaneously by adsorption of labile U, $[U]_t$ is the U^{VI} concentration in solution at time t and k_a and k_b are the forward and reverse rate constants describing slower time-dependent U^{VI} sorption. The Microsoft Excel Solver tool was used to predict the parameters $[U_o]$, k_a and k_b by minimising the sum of proportional error squared (SPES).

It should be noted that, in allowing for instantaneous adsorption of U^{VI} ions, $[U]_o$ differs from U_{added}. The model-fitted concentrations of U in solution at zero time, $[U_o]$, for different added U^{VI} concentrations and pH values (7, 8 and 9) were used to obtain 'zero-time' Freundlich adsorption isotherm parameters k_f and n_f which are assumed to represent the equilibrium of wholly labile U^{VI} ions (Eq.3):

$$U_{ads,t=0} = k_f (U_o)^{n_f} \quad (3)$$

Where $U_{ads,t=0}$ is the concentration of labile U (µg kg^{-1}), instantaneously adsorbed, at t=0 and in equilibrium with the solution concentration (U_o). The combination of k_f and n_f and the rate constants k_a and k_b were then used to model the distribution of U^{VI} between the biochar and solution as a function of contact time.

2.2.2 Spherical diffusion model

The spherical diffusion model is based on the assumption that sorption is controlled by diffusion into uniform spherical particles of radius (r) controlled by a diffusion coefficient (D) [16-18]. It has been successfully applied to describe time-dependent sorption processes in materials, including soil [19, 20], minerals [21] activated carbon [22] and waste materials e.g. 'bottom ash' and de-oiled soya [23].

The model equation is shown in Eq.(4) [16, 17]:

$$U_t = U_o\left(\frac{6}{\pi^2}\sum_{n=1}^{n=\infty}\frac{1}{n^2}\exp-\left(\frac{n^2\pi^2 Dt}{r^2}\right)\right) \tag{4}$$

where n is an integer, D is the intra-aggregate diffusion coefficient (m^2 d^{-1}) and r is the aggregate radius. Equation 4 was fitted to the time-dependent U adsorption data by optimising the compound parameter D/r^2 to minimise the SPES. Again, it is important to make a distinction between U_{added} and U_o in that some instantaneous adsorption of labile U^{VI} ions is assumed.

2.3 Isotopic exchange with $^{233}U^{VI}$ to determine $^{238}U^{VI}$ E-values ($^{238}U_E$)

Isotopic dilution (ID) has been widely used to measure the isotopically exchangeable, or 'labile', pool of an element in soils/sediments. The procedure involves spiking a geocolloidal suspension with a small quantity of an enriched minor isotope of the element of interest. The introduced spike isotope ($^{233}U^{VI}$) should behave in an identical way to the natural isotope under consideration ($^{238}U^{VI}$) but mix only with the labile pool of metal present [24-26].

At the end of the adsorption experiment (equilibrated for 7 days) selected biochar suspensions with added ^{238}U concentrations (U_{added}) of 2, 3 and 5 mg L^{-1}, and with the full range of pH values, were chosen for spiking with ^{233}U to measure the labile pool of $^{238}U^{VI}$. Suspensions spiked with $^{233}U^{VI}$ were returned to the shaker at 25 ^{o}C and sub-samples collected at 1, 2, 3, 4, 5, 6 and 8 days to investigate the effect of ^{233}U isotope mixing time on the measurement of isotopically exchangeable ^{238}U. The $^{233}U/^{238}U$ ratio in solution was determined on filtered (<0.2 µm) supernatant solutions. The apparent concentration of isotopically exchangeable ^{238}U ($^{238}U_E$; mg kg^{-1}) was calculated to establish the extent of $^{233}U \rightleftharpoons {}^{238}U$ isotope mixing on the biochar and thus the apparent lability of the added ^{238}U, as shown in Eq.(5):

$$^{238}U_E = {}^{238}U_{soln}\left[K_d + \frac{V_{total}}{W_{solid}}\right] \tag{5}$$

Where $^{238}U_{soln}$ is the concentration (mg L^{-1}) of ^{238}U in the solution of an equilibrated spiked suspension, K_d is the distribution coefficient of a ^{233}U spike (L kg^{-1}), V_{total} is the total volume (L) of suspension and W_{solid} (kg) is the weight of biochar in the suspension. The *lability* of the ^{238}U in the system can be expressed as a proportion (%) of added U ($\%^{238}U_E$).

2.4 Desorption experiment

Prior to measuring desorption, U^{VI} was allowed to adsorb on biochar for 15 d at added U^{VI} concentrations of 2, 3 and 5 mg L^{-1}. A Freundlich equation was fitted to the adsorbed data. Bespoke desorbing solutions were prepared by pre-equilibrating samples of biochar in 0.01 M $Ca(NO_3)_2$ and filtering the suspension to prepare a solution that was as close as possible to the suspensions equilibrated with U. Suspensions were allowed to equilibrate in 0.01 M $Ca(NO_3)_2$ for the same period of time and under the same conditions of pH and temperature as the U-spiked suspensions [27]. This approach was preferred over desorbing the in fresh 0.01 M $Ca(NO_3)_2$ solutions as any change in pH or anionic ligand (e.g. phosphate, bicarbonate) concentration could increase, or decrease, U solubility for reasons other than a simple change in U^{VI} solution concentration [28-30].

Desorption was undertaken by replacing 50% of the filtered supernatant solution with the U-free desorbing solution. The suspension was then shaken for 24 h. Before sampling the suspension was allowed to settle (30 min), filtered (<0.22 μm) and the solution acidified to 2% HNO_3 before analysis. This process was repeated for 4 days.

The amount of U^{VI} desorbed (U_{des}; μg kg^{-1}) was calculated for each desorption step from measured solution concentrations and the volume of supernatant removed [12]. The new adsorbed U concentration ($U_{ads,d}$; μg kg^{-1}) was calculated from the progressive loss of U in the desorbing solutions (ΣU_{des}) [12]. The measured solution concentration of U ($U_{soln,d}$; μg L^{-1}) was then used to calculate the 'expected' concentration of adsorbed U ($U_{ads,a}$; μg kg^{-1}), if U adsorption was completed reversible, from Frendlich parameters (k_f, n_f) fitted to the adsorption trend for 15 days. The difference between $U_{ads,d}$ and $U_{ads,a}$ represents the desorbability of the adsorbed U and can be expressed as:

$$\%U_{desorb} = \frac{\left[k_f(U_{soln,o})^{n_f} - U_{ads,d}\right]100}{k_f(U_{soln,o})^{n_f} - k_f(U_{soln,d})^{n_f}} \qquad (6)$$

Where $U_{soln,o}$ is the solution concentration of U at the end of the initial 15-day adsorption period.

2.5 Geochemical speciation model (WHAM-VII)

The geochemical speciation model WHAM-VII (Windermere Humic Aqueous Model, version 7) [31] was used to estimate the speciation and solubility of U^{VI} in the biochar suspensions. The free ion activities of metal ions present in solution e.g. Ca^{2+}, Mg^{2+} and

UO_2^{2+} were predicted and used to calculate the saturation index (SI) of potential solid phases [32]:

$$log_{10}\mathrm{SI} = log_{10}(\mathrm{IAP}/\mathrm{K_{SP}}) \tag{7}$$

Where IAP is the ion activity product for the candidate solid phase and K_{SP} is its solubility product. If the $\log_{10}$SI is >0 then the solution is supersaturated and the solid phase should be actively precipitating.

2.6 Statistical analysis

The residual standard deviation (RSD) was used to assess the performance of empirical models:

$$RSD = \sqrt{\frac{\sum_{i=1}^{n}(M_i - P_i)^2}{(n-c)}} \tag{8}$$

Where c = number of optimized constants; n = number of observations and M_i and P_i are measured and predicted results respectively.

3 Results and discussion

3.1 Biochar characterization

Biochar suspensions had a naturally high pH of 9.6. Elemental analysis (Table 1) gives a mole ratio of Ca:P of 1.50 suggesting the presence of Ca-deficient hydroxyapatite $Ca_5(PO_4)_3(OH)$ (Ca:P = 1.67). SEM images (Fig 1) showed grains were irregular in shape with a porous structure, probably originating from the original bone material.

3.2 Kinetics of U^{VI} adsorption

Reversible first order kinetic (RFO) and spherical diffusion models (SDM) were applied to describe the kinetics of U^{VI} adsorption. There was a marked initial loss of U from solution which was greatest at low pH values (Fig. 2). Thereafter, however, both models adequately described the time-dependent U^{VI} adsorption trends (Fig. 2).

Initial U^{VI} concentrations in solution (U_o), rate constant parameters of the RFO model (k_a and k_b) and values of D/r^2 for the SDM (Eqs 2 and 3) were all optimised independently for each combination of suspension pH and added U concentration (U_{added}); values are shown in Table 2. 'Initial U concentration' (U_o) is a fitted variable and was typically between 1–10% of the 'added U concentration (U_{added})' (Table 2) as a result of instantaneous U adsorption by the biochar. Thus the majority of the U was adsorbed very rapidly and this was followed by a slower continuing adsorption reaction (Fig. 2), limited either by reaction rate or diffusion within the biochar structure [33]. Values of k_a were much greater than k_b, especially at low pH and U concentrations. The diffusion parameter D/r^2 varied with pH and U concentration; averaged across the added U range it was maximal at pH 6 (0.0673 d^{-1}) and across the pH range was greatest at the lowest U concentration (0.0665 d^{-1}). An exact physical meaning of D/r^2 is compromised by the irregularity of the biochar particles and their variable particle size (Fig. 1); changes in U speciation with pH will also affect the values of the effective diffusion coefficient (D) and U_o.

An attempt was made to describe and predict the sorption of U^{VI} into biochar by integrating the experimental data into a predictive model that described both the initial adsorption and the subsequent time–dependent reaction. Freundlich isotherm constants (K_f and n_f) were estimated from values of U_o, determined from optimisation of the RFO model (Figure 3). This describes the U solid $\rightleftharpoons$ solution equilibrium at zero time, prior to any time-dependent adsorption or fixation of U. Thus, it can also be taken, more generally, as a description of the solid$\rightleftharpoons$solution equilibrium of *labile* U^{VI} ions. The resulting Freundlich parameters for labile U^{VI} were then used, in combination with the mean values (d^{-1}) of the rate constants (k_a and k_b), in an iterative solution, to predict time-dependent U^{VI} adsorption on biochar at pH 7, 8 and 9 from zero time to 15 days

(Fig. 4). This approach provided a good overall representation of the kinetics of U^{VI} adsorption on biochar (Fig. 4) but was only successful within a pH range (7 – 9) in which adsorption, rather than precipitation, appeared to control U retention in the solid phase.

3.3 Isotope dilution

Time-dependent adsorption may signify diffusion-limited access to otherwise labile adsorption sites or a fixation reaction e.g. crystallization, or solid-phase diffusion which liberates new surface adsorption sites. Simply measuring adsorption of $^{238}U^{VI}$ does not determine the 'reactivity' of the adsorbed U. Thus, E-values ($^{238}U_E$, Eq. 4) were measured in an attempt to estimate the isotopically exchangeable ^{238}U in the suspensions. Values of $^{238}U_E$ were determined for suspensions containing U_{added} concentrations of 2, 3 and 5 mg L^{-1} and at all six pH values following $^{238}U^{VI}$ adsorption for 7 days. However, the short adsorption times being examined (up to 7 days) presents a problem for interpretation of $^{238}U_E$ because the isotopic equilibration time normally allowed is typically 2 or 3 days (Ahmed et al., 2006). Furthermore, the combination of biochar as adsorbent and an enriched isotope of U (^{233}U) as tracer has not previously been investigated in this context. Therefore, we tested several $^{233}U^{VI}$ isotope equilibration times, including 1-6 and 8 days. Figure 5 shows that $\%^{238}U_E$ increased with isotope equilibration time up to day 4 or 5. This increase in (apparent) E-value can be attributed to slow mixing of the tracer isotope ($^{233}U^{VI}$) into less labile pools of ^{238}U and suggests the presence of slowly reactive adsorbed ^{238}U fractions on the biochar. After day 5 the measured $\%^{238}U_E$ tended towards an asymptote corresponding to about 50 – 75% of the adsorbed ^{238}U depending on the suspension pH. The trend was highly scattered for pH values of 4.5–7 reflecting low precision due to very low concentrations of ^{233}U in solution but was clearer for pH 8 and 9 where carbonate complex formation maintained a higher U concentration in solution.

The $^{238}U^{VI}$ added to the system was not in true equilibrium at the time of spiking with $^{233}U^{VI}$ as shown by the time-dependent adsorption (Figures 2 and 4). This compromises measurement of $^{238}U_E$ to some degree, but the change in solution and solid phase concentrations of ^{238}U were proportionately small between contact times of 7 and 15 days (the time period tested with ^{233}U equilibration). Therefore a more realistic interpretation of the ^{233}U equilibration data in Fig. 5 is that they genuinely reflect the slow reaction kinetics of adsorbed ^{238}U but also suggest that the majority of recently adsorbed ^{238}U remains isotopically exchangeable within a period of several days.

3.4 Desorption of $^{238}U^{VI}$

To further assess the lability of adsorbed ^{238}U, sequential desorption of ^{238}U was investigated. This followed immediately after the adsorption process, as a series of desorption steps using a U-free solution prepared in a similar way to the adsorption suspensions described previously. Four 1-day cycles of desorption were undertaken, (Figure 6), following an initial reaction time (adsorption) of 15 days. The general trend in Fig. 6 displays substantial adsorption hysteresis with desorption of U^{VI} following a markedly different trend from the original adsorption process with poor buffering of the solution concentration. Desorbability ($\%U_{desorb}$; Eq.6) of adsorbed U^{VI} (Table 4) was assessed after the fourth 24 h desorption cycle. Values of $\%U_{desorb}$ were very low for pH ≥6 with an average of 6.0±0.7 % across all U concentrations and pH values. For pH 9, the adsorbed U was more strongly buffered with an average value for $\%U_{desorb}$ of 23±2.1 %. Direct comparison of $\%^{238}U_E$ and $\%U_{desorb}$ is conceptually valid as the latter should represent the proportion of adsorbed U which is capable of responding to a change in equilibrium with the solution phase. Values of $\%^{238}U_E$ include U in solution but this is a trivial proportion of the total labile pool. For pH 6, 7 and 8 values of $\%U_{desorb}$ were substantially lower than $\%^{238}U_E$ for an equivalent 1 day isotopic equilibration (Figure 5). This may reflect the greater contact time (15 d) prior to desorption compared to the initial E-value measurement following 7 d adsorption. For pH 9, the two indices of U lability were much closer, both measurements probably reflecting the influence of carbonate complex formation in retaining adsorbed U in a more labile, reactive state.

3.5 U^{VI} speciation and stability diagram

To assess the likelihood of U precipitation contributing to the apparent fixation of U, chemical speciation of U^{VI} in the suspensions was calculated using WHAM-VII. Saturation indices for possible U-containing solid phases (Table 3) were calculated from predicted free ion activities of calcium, carbonate, magnesium, phosphate and uranium at pH values of 4.5, 5, 6, 7, 8 and 9, adsorption times of 1-5 d and 7 d and initial U^{VI} concentrations of 0.1, 0.5, 1, 2, 3 and 5 mg L^{-1}.

Saturation indices (Annex 2) suggest that autunite was oversaturated (precipitated or co-precipitated) at low pH (<6). Our modelling observations are consistent with the findings of a number of published papers that have attempted to identify U phases formed using a range of techniques and greater U concentrations. In a study by Beazley et al. (2007) modelling a synthetic groundwater system they identified low U solubility with autunite formation in the pH range 4-8 [34]. Fuller et al. (2002) investigated the reaction between synthetic hydroxyapatite and uranium using batch experiments in the pH range 6.3-6.9 and identified the solid phases formed using SEM, synchrotron XRD and XAS [35]. Autunite formation was observed only at pH 6.3 in agreement with the observation in our study of autunite precipitation at pH < 6.5. Singh et al. (2012) also identified a surface precipitate of U-phosphate (autunite) in experiments investigating U(VI) immobilization by goethite in the presence of phosphate [36]. At higher pH values

(≥7; current study) there was oversaturation of swartzite, bayleyite and liebigite. This suggests that U^{VI} uptake by biochar is not only controlled by adsorption reactions but also by precipitation reactions, depending on the pH range - a similar conclusion to that of a study on UO_2^{2+} adsorption on hydroxyapatite [37]. Mehta et al (2016) used batch experiments to assess the extent of U(VI) immobilization by calcium and phosphate over a range of pH 4-7.5 and also observed autunite formation at pH 4 and 6 with U(VI) sorbed on Ca-PO_4 solid phases at pH 7.5 or structurally incorporated into amorphous calcium phosphate phases where sufficient dissolved calcium and phosphate were available [38].

Precipitation could also explain the slow reaction kinetics, time-dependent sorption, poor desorbability and non-isotopic exchangeability of U adsorbed on the biochar. Interpolated model lines for predicted solid phases are shown in Fig 7 using free ion activities calculated at each pH value from the WHAM VII speciation model. It is evident that solubility of UO_2^{2+} was governed by autunite [$Ca(UO_2)_2(PO_4)_2.10H_2O$] at pH 4.5, 5.0 and 6.0. The dominant solid phases at higher pH appear to be swartzite, bayleyite and liebigite as suggested in other studies [39, 40].

4 Conclusions

In this work, we demonstrated the time-dependent fixation of U^{VI} from aqueous solution into biochar produced by gasification of cow bones. Fixation of U^{VI} on biochar exhibited rapid adsorption on the reactive groups on biochar surfaces followed by a slower reaction rate suggesting that the U^{VI} may gradually penetrate the porous structure of biochar grains or form progressively stronger surface complexes or new, less soluble, solid phases. The suggestion that the slow adsorption reaction reflected a 'fixation' reaction was supported by measurement of isotopically exchangeable ^{238}U with ^{233}U, slow isotopic equilibration over several days, poor desorbability, especially at low pH values and a test of ion activity products which suggested the formation of new U-containing solid phases. Speciation of U^{VI} solid phases predicted from WHAM-VII showed that the controlling solid phase at pH 4.5-6 was autunite while at higher pH (7-9) the controlling solid phases were swartzite, bayleyite and liebigite.

Biochar with a high hydroxyl-apatite content is an efficient adsorbent for U^{VI} ions over a wide range of pH. It may be suitable for treatment of contaminated low level waste streams due to its substantial capacity for desorption hysteresis below pH 7. It may also be suitable as a soil amendment in the pH range 6 -7 due to poor apatite solubility in this pH range combined with limited carbonate complexation of U^{VI} ions.

Acknowledgements

The authors acknowledge funding from the Egyptian Atomic Energy Authority and Higher Education Ministry of Egypt. Lorraine Field is thanked for help with SEM photography. Helen West is thanked for supplying the biochar. Published with permission of the Executive Director, British Geological Survey.

Table 1: Elemental composition of biochar.

Table 2: Kinetic rate constants (k_a, k_b; d^{-1}) for the reversible first order model and the parameter D/r^2 (d^{-1}) for the spherical diffusion model. The variable U_0 (μg L^{-1}) is the extrapolated U concentration in solution at zero time.

Table 3: Solubility products of selected U phases.

Table 4: Adsorbed U^{VI} (U_{ads}; mg kg^{-1}) and desorbability ($\%U_{desorb}$; Eq.6) of U from biochar after 15 days contact at different pH and initial U^{VI} concentrations (2, 3 and 5 mg L^{-1}) calculated following four successive 24 h desorption cycles.

Table 1: Elemental composition of biochar.

Element	Concentration (mg kg^{-1})	Element	%
B	1.52	C	6.75 $\pm$ 0.293
Na	3830	Inorg-C	0.601 $\pm$ 0.007
Mg	4040	N	0.479 $\pm$ 0.042
P	113000	H	0.404 $\pm$ 0.023
S	1660		
K	751	Moisture Content	0.896 $\pm$ 0.088
Ca	219000	LOI	10.3 $\pm$ 0.085
Ti	91.3		
Al	1250		
V	0.332		
Cr	0.371		
Mn	11.1		
Fe	125		
Co	0.0831		
Ni	0.682		
Cu	1.19		
Zn	26.4		
As	0.0821		
Se	0.0313		
Rb	1.86		
Sr	316		
Ag	0.0113		
Cd	0.0901		
Cs	0.0703		
Ba	142		
Pb	0.721		

Table 2: Kinetic rate constants (k_a, k_b; d^{-1}) for the reversible first order model and the parameter D/r^2 (d^{-1}) for the spherical diffusion model. The variable U_0 ($\mu g\ L^{-1}$) is the extrapolated U concentration in solution at zero time.

U_{added} ($\mu g\ L^{-1}$)		**Reversible First Order Model**							**Spherical Diffusion Model**					
	pH:	**4.5**	**5**	**6**	**7**	**8**	**9**	**pH :**	**4.5**	**5**	**6**	**7**	**8**	**9**
	U_0 ($\mu g\ L^{-1}$)	**1.014**	**1.60**	**1.020**	**1.30**	**5.48**	**1.12**	**U_0 ($\mu g\ L^{-1}$)**	**1.80**	**2.45**	**1.28**	**2.20**	**7.29**	**1.49**
100	**K_a**	0.776	1.29	1.05	0.369	0.430	0.365	**D/r^2**	0.0854	0.125	0.0884	0.0415	0.0319	0.0267
	K_b	0.000331	0.000256	0.000276	0	0.0389	0.0380							
	R^2	0.988	0.999	0.965	0.950	0.991	0.979	**R^2**	0.992	0.999	0.976	0.970	0.973	0.963
	U_0 ($\mu g\ L^{-1}$)	**5.65**	**7.47**	**5.13**	**8.54**	**34.6**	**12.6**	**U_0 ($\mu g\ L^{-1}$)**	**9.42**	**12.0**	**8.11**	**12.3**	**43.8**	**14.8**
500	**K_a**	0.811	1.10	0.845	0.391	0.416	0.485	**D/r^2**	0.0821	0.109	0.0841	0.0333	0.0277	0.0284
	K_b	0.0155	0.00700	0.0000688	0.0271	0.0507	0.0660							
	R^2	0.983	0.999	0.998	0.964	0.979	0.977	**R^2**	0.983	0.999	0.997	0.961	0.948	0.926
	U_0 ($\mu g\ L^{-1}$)	**12.2**	**7.32**	**9.32**	**13.8**	**72.6**	**43.5**	**U_0 ($\mu g\ L^{-1}$)**	**17.1**	**10.5**	**13.7**	**21.05**	**90.1**	**54.0**
1000	**K_a**	0.866	0.532	0.844	0.418	0.442	0.518	**D/r^2**	0.0720	0.0487	0.0794	0.0391	0.0285	0.0340
	K_b	0.0319	0.000650	0.0000496	0.0211	0.0554	0.0556							
	R^2	0.990	0.984	0.994	0.952	0.977	0.983	**R^2**	0.982	0.983	0.995	0.956	0.941	0.946
	U_0 ($\mu g\ L^{-1}$)	**16.2**	**6.97**	**9.96**	**29.9**	**143**	**125**	**U_0 ($\mu g\ L^{-1}$)**	**22.5**	**9.59**	**13.6**	**46.5**	**180**	**139**
2000	**K_a**	0.499	0.297	0.615	0.358	0.406	0.697	**D/r^2**	0.0425	0.0250	0.0528	0.0351	0.0265	0.0399
	K_b	0.0126	0.00683	0.00553	0.0144	0.0530	0.0706							
	R^2	0.982	0.998	0.978	0.950	0.973	0.977	**R^2**	0.982	0.984	0.980	0.960	0.941	0.914
	U_0 ($\mu g\ L^{-1}$)	**14.4**	**6.57**	**12.9**	**49.4**	**202**	**238**	**U_0 ($\mu g\ L^{-1}$)**	**19.1**	**9.40**	**15.2**	**76.5**	**256**	**261**
3000	**K_a**	0.255	0.225	0.646	0.463	0.392	0.717	**D/r^2**	0.0203	0.0203	0.0489	0.0436	0.0262	0.04044
	K_b	0.00738	0.00605	0.00963	0.0237	0.0504	0.0713							
	R^2	0.991	0.951	0.881	0.957	0.967	0.983	**R^2**	0.980	0.959	0.888	0.959	0.938	0.919
	U_0 ($\mu g\ L^{-1}$)	**13.4**	**6.97**	**10.6**	**96.2**	**296**	**497**	**U_0 ($\mu g\ L^{-1}$)**	**17.8**	**9.40**	**14.02**	**149**	**364**	**573**
5000	**K_a**	0.143	0.178	0.621	0.511	0.367	0.702	**D/r^2**	0.0115	0.0148	0.0502	0.0493	0.0228	0.0430
	K_b	0	0	0.0194	0.00848	0.0544	0.0634							
	R^2	0.976	0.970	0.950	0.997	0.977	0.983	**R^2**	0.981	0.972	0.947	0.997	0.942	0.932

Table 3: Solubility products of selected U phases.

Mineral phase	Dissolution reaction	Log K_{sp}	Reference
Swartzite $CaMgUO_2(CO_3)_3.12(H_2O)$	$CaMgUO_2(CO_3)_3(H_2O)_{12} \leftrightarrows Ca^{2+} + Mg^{2+} + UO_2^{2+} + 3CO_3^{2-} + 12H_2O$	-37.9	[41]
Bayleyite $Mg_2UO_2(CO_3).18(H_2O)$	$Mg_2UO_2(CO_3)_3(H_2O)_{18} \leftrightarrows 2Mg^{2+} + UO_2^{2+} + 3CO_32- + 18H_2O$	-36.6	[41]
Liebigite $Ca_2UO_2(CO_3)_3.10(H_2O)$	$Ca_2UO_2(CO_3)_3(H_2O)_{10} \leftrightarrows 2Ca^{2+} + UO_2^{2+} + 3CO_3^{2-} + 10H_2O$	-36.9	[41]
Rutherfordine UO_2CO_3	$UO_2CO_3 \leftrightarrows UO_2^{2+} + CO_3^{2-}$	-13.89	[41]
Metaschoepite $UO_2(OH)_2 \cdot 2(H_2O)$	$2H^+ + UO_3(H_2O)_2 \leftrightarrows UO_2^{2+} + 3H_2O$	5.52	[42]
Uranyl orthophosphate $(UO_2)_3(PO_4)_2.4(H_2O)$	$(UO_2)_3(PO_4)_2(H_2O)_4 \leftrightarrows 3UO_2^{2+} + 2PO_4^{3-} + 4H_2O$	-49.36	[43]
Uranyl hydrogen phosphate $UO_2HPO_4.(H_2O)_3$	$UO_2HPO_4.(H_2O)_3 \leftrightarrows UO_2^{2+} + HPO_4^{2-} + 3H_2O$	-13.17	[43]
Autunite $Ca(UO_2)_2(PO_4)_2.(H_2O)_3$	$Ca(UO_2)_2(PO_4)_2.(H_2O)_3 \leftrightarrows Ca^{2+} + 2UO_2^{2+} + 2PO_4^{3-} + 3H_2O$	-48.36	[43]

Table 4: Adsorbed U^{VI} (U_{ads}; mg kg^{-1}) and desorbability ($\%U_{desorb}$; Eq.6) of U from biochar after 15 days contact at different pH and initial U^{VI} concentrations (2, 3 and 5 mg L^{-1}) calculated following four successive 24 h desorption cycles.

Added U^{VI}	**pH**							
	6		**7**		**8**		**9**	
	U_{ads}	$\%U_{desorb}$	U_{ads}	$\%U_{desorb}$	U_{ads}	$\%U_{desorb}$	U_{ads}	$\%U_{desorb}$
mg L^{-1}	mg kg^{-1}	%	mg kg^{-1}	%	mg kg^{-1}	%	mg kg^{-1}	%
2	39.3	14	39.4	5.3	39.5	6.9	39.7	24
3	59.1	3.8	58.9	9.1	59.4	9.2	59.4	19
5	98.4	4.0	98.5	4.5	98.9	7.6	98.8	26

Figure 1: Scanning electron micrographs of bone biochar.

Figure 2: Effect of pH and contact time on U concentration in biochar suspensions. Lines represent optimnised fits of the reversible first order reaction model ——— and spherical diffsion model ------ fitted independently to data for each added U^{VI} concentration: ♦ U_0=0.1 mg L^{-1}, ■ U_0=0.5 mg L^{-1}, ▲ U_0=1 mg L^{-1}, ● U_0=2 mg L^{-1}, ◇ U_0=3 mg L^{-1}, □ U_0=5 mg L^{-1}.

Figure 3: Zero time Freundlich isotherms at different pH (♦ pH= 7, ■ pH= 8, ▲ pH= 9) predicted from reversible first order kinetics.

Figure 4: Time-dependent adsorption isotherms for U^{VI} on biochar for equilibration times (days) of: zero (•), 1 (♦), 2 (■), 3 (▲), 4 (●), 5 (◇), 7 (□), 15 (Δ). Instantaneous adsorption (•) was estimated from the 'zero time' Freundlich isotherm parameters (Figure 3); the model lines shown were calculated from average values of the reversible first-order kinetic model parameters k_a and k_b.

Figure 5: U lability (%E-value) at different added U^{VI} concentrations (● U_0=2 mg L^{-1}, ◇ U_0=3 mg L^{-1}, □ U_0=5 mg L^{-1}) as a function of total adsorbed U^{VI} on biochar.

Figure 6: Uranium (U^{VI}) desorbed from biochar at different pH values; ♦ = adsorption (15 days), and desorption ◇ = 1 day, △ = 2 days, □ = 3 days and ○ = 4 days.

Figure 7: Stability diagram showing predicted solid phases formed during adsorption of uranyl ions (UO_2^{2+}) onto biochar over 1-5 and 7 days at six initial U_o concentrations (□ U_0=0.1 mg L^{-1}, ◇ U_0 = 0.5 mg L^{-1}, Δ U_0=1 mg L^{-1}, o U_0=2 mg L^{-1}, x U_0 =3 mg L^{-1} and + U_0=5 mg L^{-1}) and six pH values (4.5, 5, 6, 7, 8 and 9).

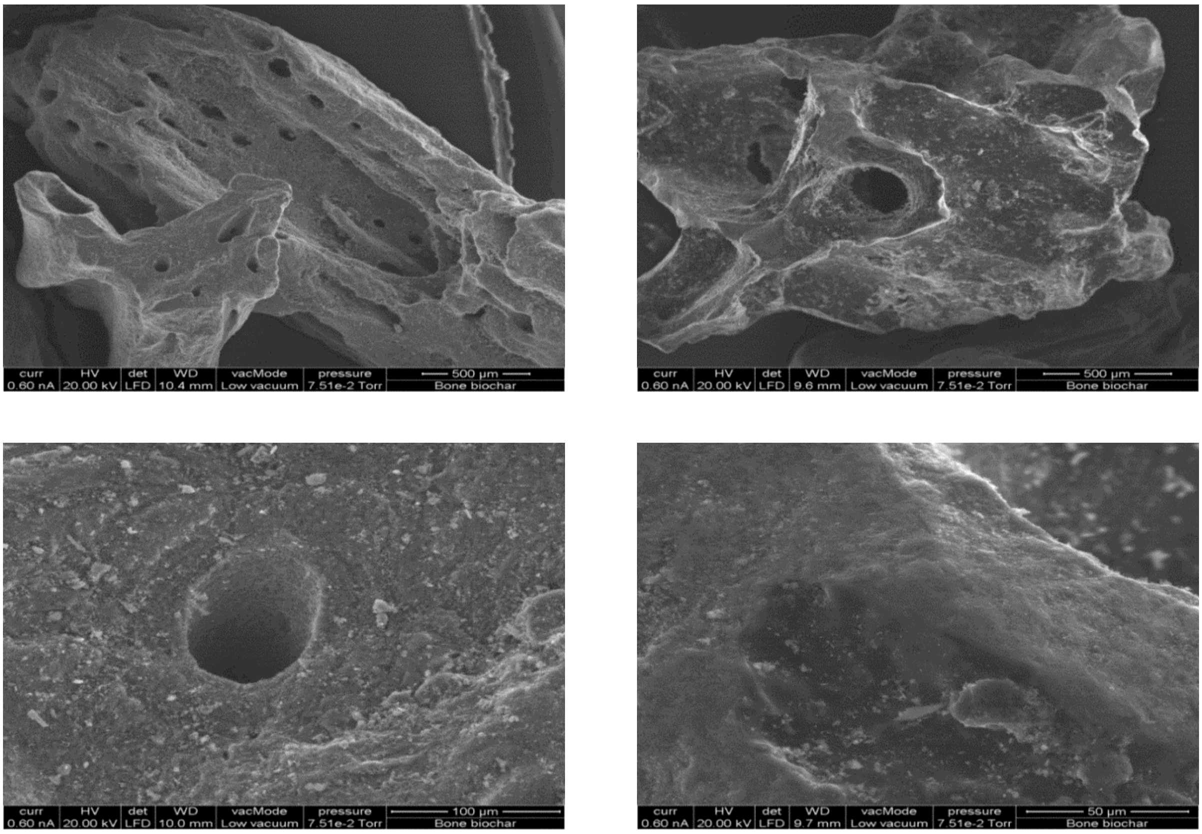

Figure 1: Scanning electron micrographs of bone biochar.

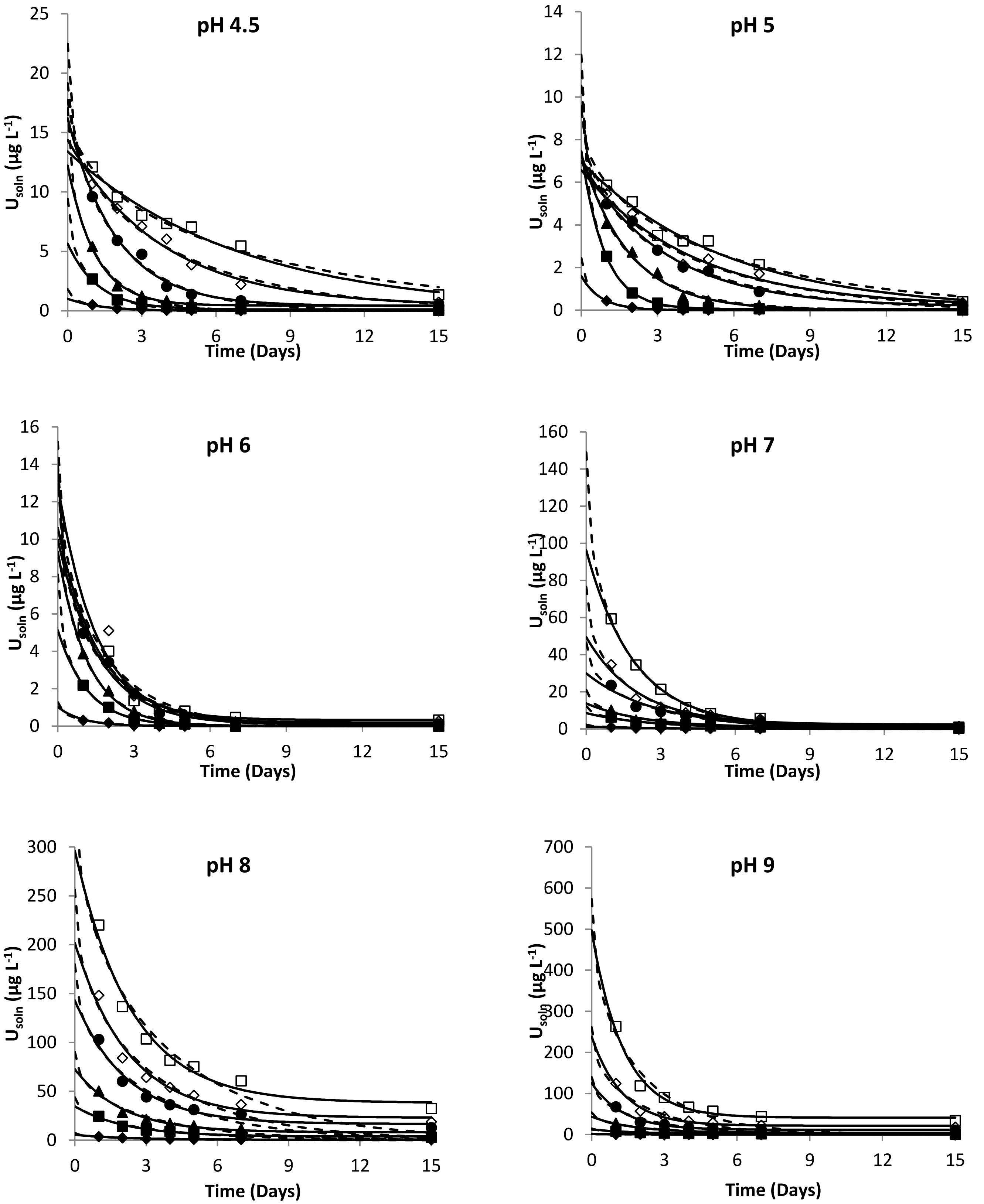

Figure 2: Effect of pH and contact time on U concentration in biochar suspensions. Lines represent optimnised fits of the reversible first order reaction model ——— and spherical diffusion model ------ fitted independently to data for each added U^{VI} concentration: ♦ U_0=0.1 mg L^{-1}, ■ U_0= 0.5 mg L^{-1}, ▲ U_0=1 mg L^{-1}, ● U_0=2 mg L^{-1}, ◇ U_0=3 mg L^{-1}, □ U_0=5 mg L^{-1}.

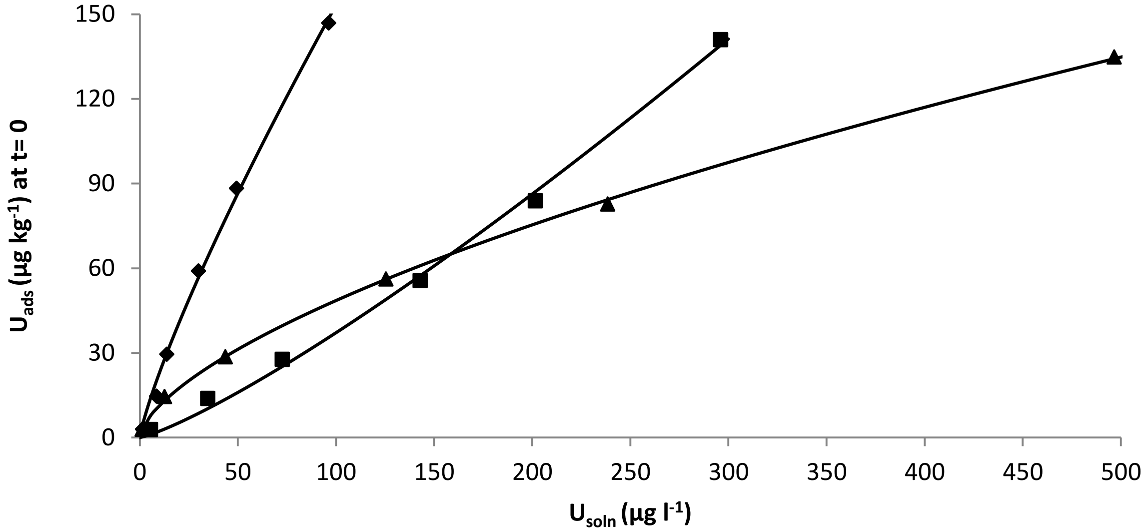

Figure 3: Zero time Freundlich isotherms at different pH (♦ pH= 7, ■ pH= 8, ▲ pH= 9) predicted from reversible first order kinetics.

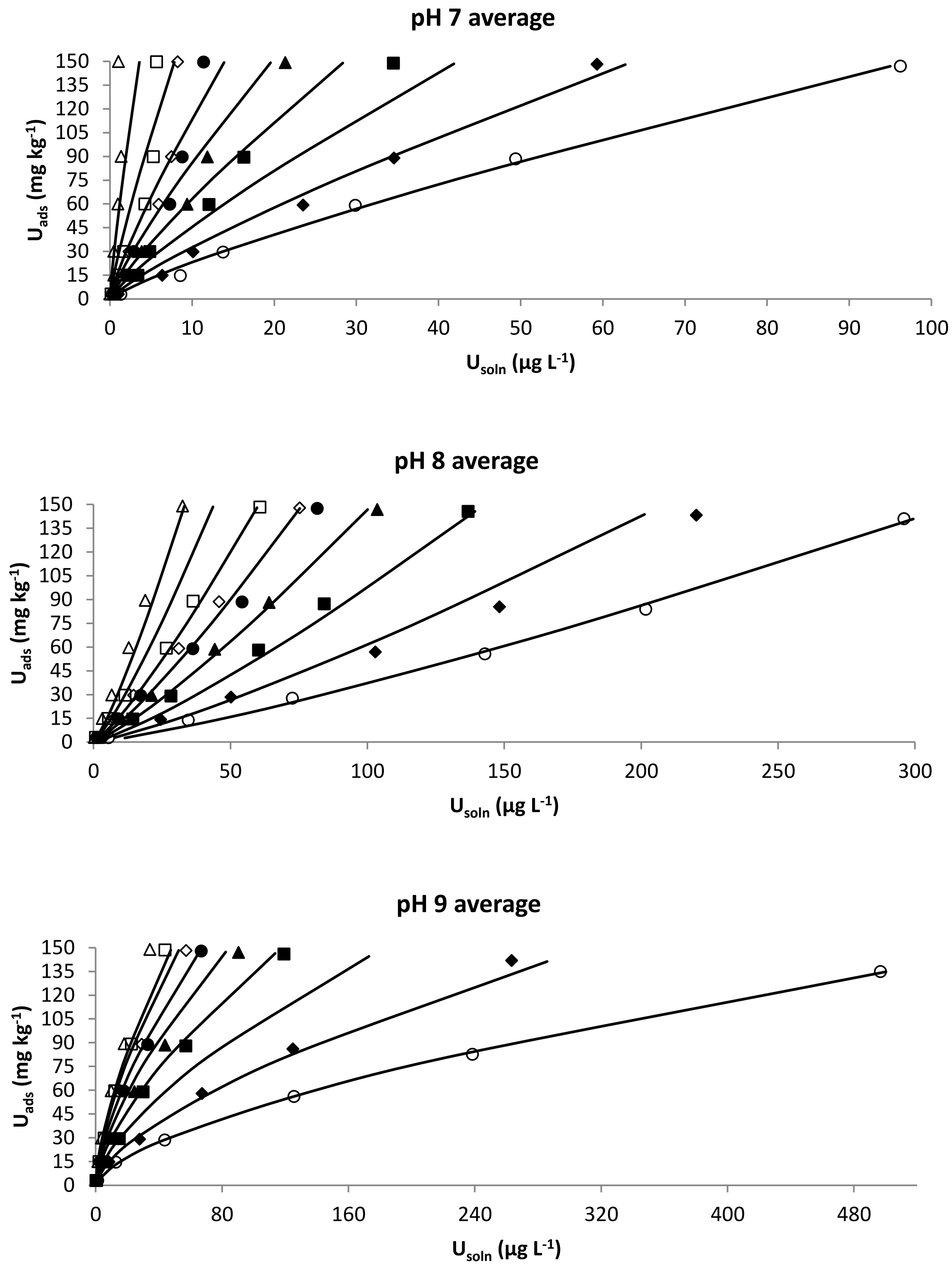

Figure 4: Time-dependent adsorption isotherms for U^{VI} on biochar for equilibration times (days) of: zero (•), 1 (♦), 2 (■), 3 (▲), 4 (●), 5 (◇), 7 (□), 15 (△). Instantaneous adsorption (•) was estimated from the 'zero time' Freundlich isotherm parameters (Figure 3); the model lines shown were calculated from average values of the reversible first-order kinetic model parameters k_a and k_b.

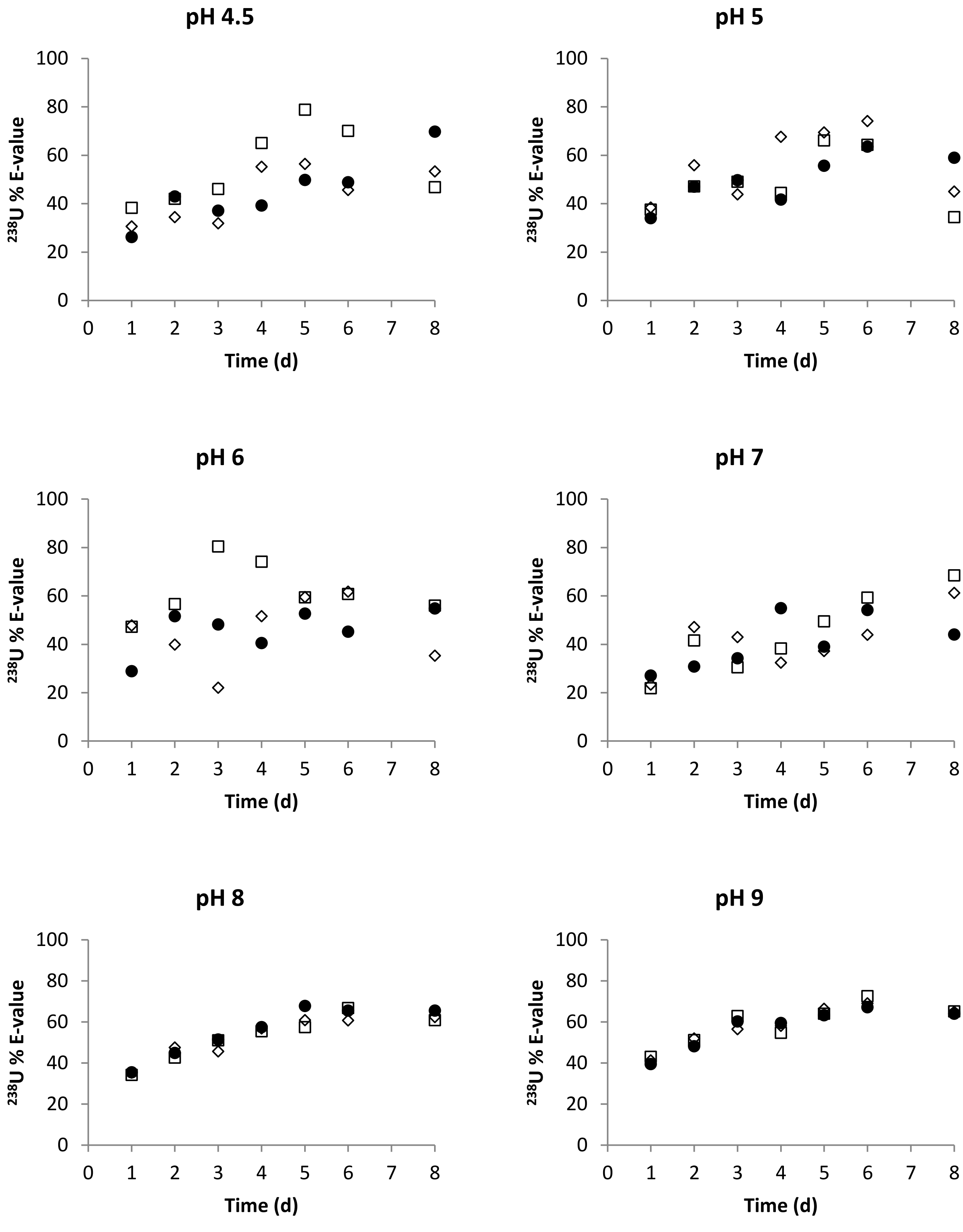

Figure 5: U lability (%E-value) at different added U^{VI} concentrations (● U_0= 2 mg L^{-1}, ◊ U_0= 3 mg L^{-1}, □ U_0= 5 mg L^{-1}) as a function of total adsorbed U^{VI} on biochar.

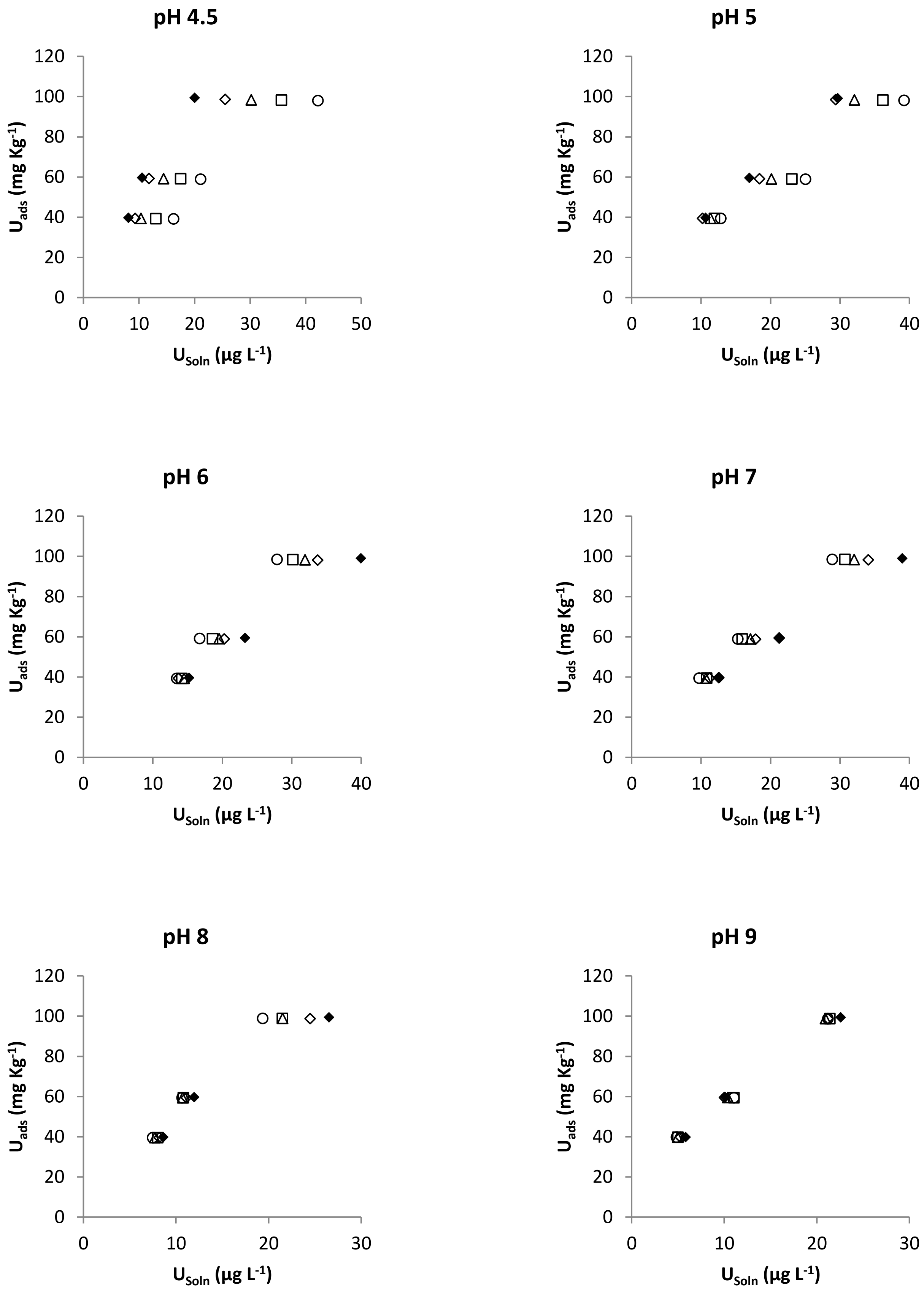

Figure 6: Uranium (U^{VI}) desorbed from biochar at different pH values; ♦ = adsorption (15 days), and desorption ◊ = 1 day, △ = 2 days, , □ = 3 days and ○ = 4 days.

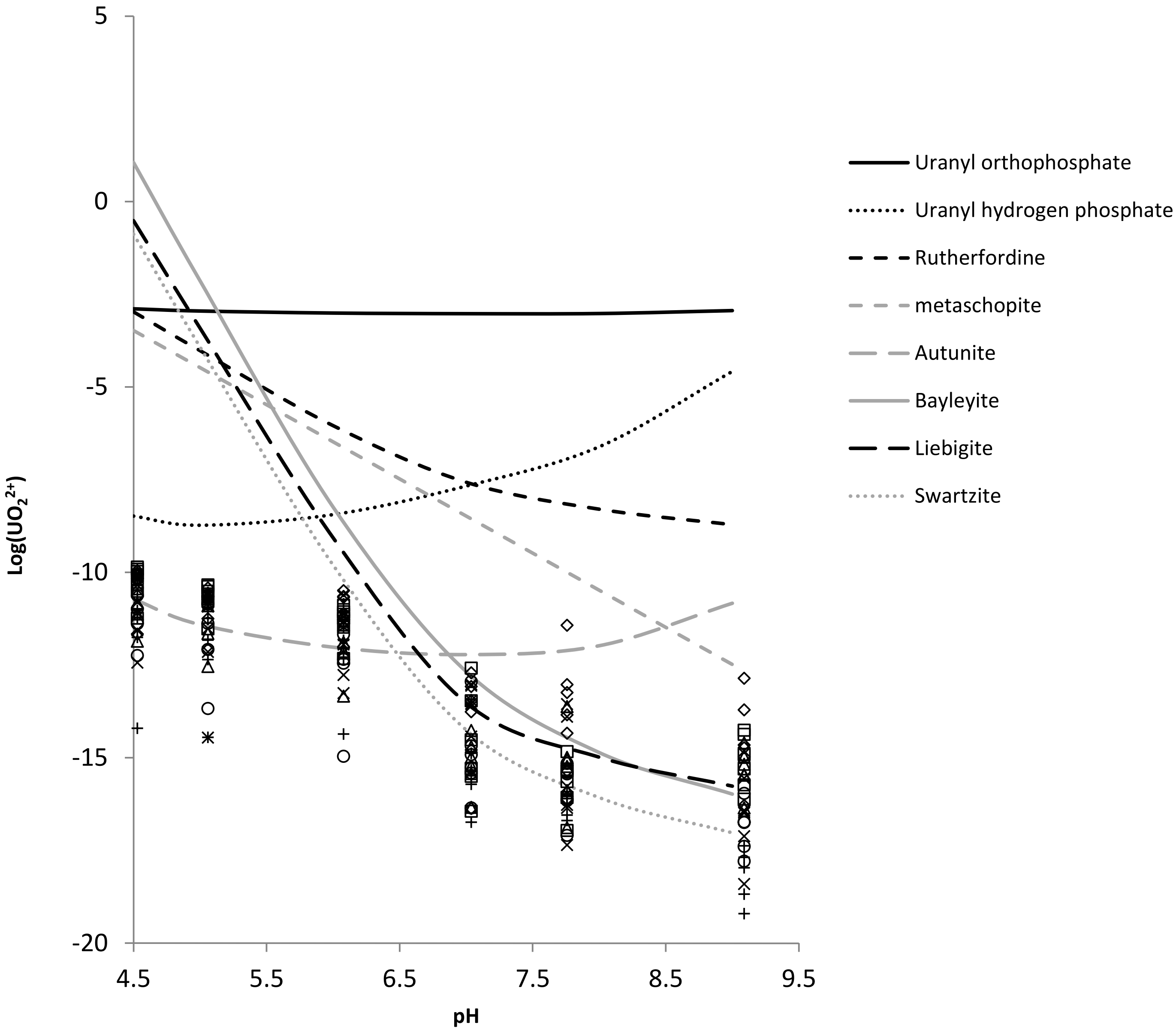

Figure 7: Stability diagram showing predicted solid phases formed during adsorption of uranyl ions (UO_2^{2+}) onto biochar over 1-5 and 7 days at six initial U_o concentrations (□ U_0 = 0.1 mg L^{-1}, ◇ U_0 = 0.5 mg L^{-1}, Δ U_0 = 1 mg L^{-1}, o U_0 = 2 mg L^{-1}, x U_0 = 3 mg $L^{-1}$and + U_0 = 5 mg L^{-1}) and six pH values (4.5, 5, 6, 7, 8 and 9).

Electronic Annex 1: Saturation indices of solid phases that may form during U^{VI} adsorption on biochar.

pH	Time (d)	Swartzite $CaMgUO_2(CO_3)_3.12(H_2O)$						Bayleyite $Mg_2UO_2(CO_3).18(H_2O)$						Liebigite $Ca_2UO_2(CO_3)_3.10(H_2O)$					
		Initial concentration (mol L^{-1} x 10^{-6}) of U in biochar suspension																	
		0.42	2.10	4.20	8.40	12.6	21.0	0.42	2.10	4.20	8.40	12.6	21.0	0.42	2.10	4.20	8.40	12.6	21.0
4.5	1	-9.97	-9.30	-8.99	-8.81	-9.23	-8.74	-9.45	-8.77	-8.47	-8.31	-8.71	-8.22	-8.44	-7.75	-7.46	-7.28	-7.69	-7.21
	2	-9.30	-8.99	-8.81	-9.23	-8.74	-10.94	-8.77	-8.47	-8.31	-8.71	-8.22	-10.41	-7.75	-7.46	-7.28	-7.69	-7.21	-9.41
	3	-8.99	-8.81	-9.23	-8.74	-10.94	-10.23	-8.47	-8.31	-8.71	-8.22	-10.41	-9.70	-7.46	-7.28	-7.69	-7.21	-9.41	-8.69
	4	-8.81	-9.23	-8.74	-10.94	-10.23	-9.88	-8.31	-8.71	-8.22	-10.41	-9.70	-9.36	-7.28	-7.69	-7.21	-9.41	-8.69	-8.36
	5	-9.23	-8.74	-10.94	-10.23	-9.88	-9.51	-8.71	-8.22	-10.41	-9.70	-9.36	-8.99	-7.69	-7.21	-9.41	-8.69	-8.36	-7.97
	7	-8.74	-10.94	-10.23	-9.88	-9.51	-9.29	-8.22	-10.41	-9.70	-9.36	-8.99	-8.79	-7.21	-9.41	-8.69	-8.36	-7.97	-7.78
5	1	-7.80	-6.51	-6.31	-6.33	-6.70	-6.21	-9.67	-8.36	-8.18	-8.21	-8.57	-8.06	-8.24	-6.95	-6.74	-6.74	-7.13	-6.66
	2	-8.19	-7.35	-6.81	-6.74	-6.74	-6.54	-10.1	-9.20	-8.67	-8.61	-8.60	-8.39	-8.63	-7.80	-7.25	-7.16	-7.17	-6.99
	3	-8.83	-7.88	-7.26	-7.03	-6.92	-6.88	-10.7	-9.73	-9.12	-8.90	-8.78	-8.72	-9.28	-8.33	-7.69	-7.46	-7.36	-7.33
	4	-10.0	-8.43	-7.47	-7.16	-7.03	-6.66	-11.9	-10.3	-9.33	-9.04	-8.90	-8.51	-10.5	-8.89	-7.90	-7.58	-7.47	-7.11
	5	-10.7	-8.41	-7.80	-7.19	-6.17	-6.84	-12.6	-10.3	-9.66	-9.07	-7.03	-8.68	-11.2	-8.86	-8.24	-7.62	-7.61	-7.29
	7	-10.6	-8.32	-8.03	-7.24	-6.98	-6.96	-12.4	-10.2	-9.90	-9.13	-8.85	-8.82	-11.0	-8.76	-8.46	-7.66	-7.41	-7.41
6	1	-2.04	-1.80	-0.872	-0.794	-0.707	-0.953	-3.71	-3.40	-2.51	-2.45	-2.36	-2.61	-2.67	-2.50	-1.54	-1.44	-1.35	-1.60
	2	-2.82	-1.91	-1.92	-1.50	-1.32	-1.60	-4.48	-3.49	-3.54	-3.14	-2.96	-3.25	-3.46	-2.62	-2.60	-2.16	-1.98	-2.26
	3	-2.95	-1.90	-1.56	-0.382	-1.07	-1.51	-4.60	-3.48	-3.19	-1.02	-2.71	-3.15	-3.60	-2.62	-2.24	-2.04	-1.73	-2.17
	4	-4.83	-2.35	-2.34	-1.74	-2.15	-2.29	-6.48	-3.93	-3.96	-3.38	-3.79	-3.93	-5.47	-3.06	-3.02	-2.41	-2.82	-2.95
	5	-4.26	-2.95	-3.82	-2.34	-2.36	-1.66	-5.92	-4.53	-5.44	-3.97	-3.99	-3.30	-4.91	-3.67	-4.49	-3.00	-3.02	-2.31
	7	-5.26	-2.51	-2.23	-2.36	-2.03	-1.18	-6.91	-4.10	-3.85	-4.00	-3.67	-2.83	-5.90	-3.23	-2.91	-3.02	-2.69	-1.84
7	1	-1.24	-0.445	-0.225	0.125	0.263	0.948	-2.77	-1.96	-1.73	-1.39	-1.28	-0.593	-2.02	-1.23	-1.02	-0.661	-0.490	0.189
	2	-1.53	-0.704	-1.53	-0.153	-0.052	0.272	-3.04	-2.21	-4.02	-1.66	-1.59	-1.26	-2.33	-1.50	-1.34	-0.950	-0.819	-0.493
	3	-1.68	-0.825	-0.629	-0.254	-0.185	0.068	-3.19	-2.33	-2.11	-1.75	-1.71	-1.46	-2.48	-1.62	-1.44	-1.06	-0.956	-0.700
	4	-1.77	-0.911	-0.753	-0.368	-0.320	-0.200	-3.27	-2.41	-2.24	-1.87	-1.85	-1.73	-2.57	-1.71	-1.57	-1.17	-1.09	-0.972
	5	-1.86	-1.00	-0.849	-0.452	-0.385	-0.346	-3.36	-2.50	-2.32	-1.95	-1.91	-1.87	-2.66	-1.81	-1.67	-1.26	-1.16	-1.12
	7	-2.14	-1.16	-1.00	-0.603	-0.539	-0.509	-3.64	-2.66	-2.48	-2.11	-2.07	-2.04	-2.94	-1.96	-1.81	-1.40	-1.31	-1.27
8	1	-0.382	0.446	1.25	1.11	1.23	1.36	-1.61	-0.767	0.006	-0.072	0.022	0.108	-1.46	-0.640	0.186	-0.017	0.142	0.313
	2	-0.573	0.221	0.490	0.815	0.993	1.16	-1.79	-0.983	-0.739	-0.361	-0.208	-0.077	-1.66	-0.875	-0.580	-0.309	-0.106	0.105
	3	-0.768	0.084	0.362	0.747	0.877	1.05	-1.98	-1.12	-0.865	-0.422	-0.322	-0.196	-1.85	-1.02	-0.711	-0.384	-0.223	-0.014
	4	-0.853	0.017	0.278	0.660	1.29	0.945	-2.06	-1.19	-0.952	-0.509	0.090	-0.293	-1.94	-1.08	-0.793	-0.471	0.186	-0.117
	5	-0.951	-0.068	0.216	0.593	0.738	0.911	-2.16	-1.27	-1.00	-0.576	-0.455	-0.323	-2.04	-1.17	-0.863	-0.538	-0.368	-0.154
	7	-1.07	-0.194	0.104	0.524	0.636	0.818	-2.28	-1.40	-1.12	-0.648	-0.559	-0.420	-2.15	-1.29	-0.968	-0.605	-0.468	-0.245
9	1	-0.992	0.138	0.673	1.02	1.28	1.60	-2.06	-0.907	-0.356	-0.054	0.206	0.517	-2.22	-1.12	-0.599	-0.212	0.048	0.380
	2	-1.14	-0.225	0.359	0.652	0.601	1.22	-2.20	-1.26	-0.662	-0.407	-0.450	0.166	-2.37	-1.49	-0.920	-0.589	-0.649	-0.034
	3	-1.27	-0.250	0.271	0.581	0.845	1.16	-2.32	-1.28	-0.748	-0.481	-0.207	0.100	-2.52	-1.52	-1.01	-0.656	-0.403	-0.089
	4	-1.30	-0.322	0.159	0.464	0.744	1.06	-2.35	-1.34	-0.859	-0.586	-0.296	0.019	-2.55	-1.60	-1.12	-0.785	-0.516	-0.207
	5	-1.34	-0.358	0.119	0.424	0.693	1.45	-2.39	-1.38	-0.898	-0.623	-0.344	0.414	-2.59	1.64	-1.16	-0.830	-0.569	-0.184
	7	-1.53	-0.456	-0.011	0.308	0.589	0.884	-2.56	-1.46	-1.01	-0.728	-0.443	-0.141	-2.79	-1.75	-1.31	-0.956	-0.680	-0.391

Electronic annex 1 cont'd.

pH	Time (d)	Autunite $Ca(UO_2)_2(PO_4)_2.10H_2O$						Metaschoepite $UO_3(H_2O)_2.2H_2O$						Rutherfordine UO_2CO_3					
		Initial concentration (mol L^{-1} x 10^{-6}) of U in biochar suspension																	
		0.42	**2.10**	**4.20**	**8.40**	**12.6**	**21.0**	**0.42**	**2.10**	**4.20**	**8.40**	**12.6**	**21.0**	**0.42**	**2.10**	**4.20**	**8.40**	**12.6**	**21.0**
4.5	1	-1.03	0.435	1.06	1.58	1.65	1.76	-7.57	-6.84	-6.51	-6.30	-6.25	-6.19	-7.09	-6.37	-6.06	-5.87	-5.96	-5.76
	2	-1.92	-0.490	0.229	1.14	1.48	1.56	-7.99	-7.29	-6.96	-6.50	-6.35	-6.29	-6.37	-6.06	-5.87	-5.96	-5.76	-7.69
	3	-2.33	-0.848	-0.239	0.941	1.28	1.39	-8.19	-7.45	-7.15	-6.59	-6.41	-6.34	-6.06	-5.87	-5.96	-5.76	-7.69	-6.99
	4	-3.33	-1.38	-0.567	0.199	1.15	1.31	-8.58	-7.72	-7.32	-6.95	-6.50	-6.38	-5.87	-5.96	-5.76	-7.69	-6.99	-6.65
	5	-3.47	-1.69	-0.765	-0.147	0.761	1.29	-8.77	-7.89	-7.43	-7.14	-6.68	-6.41	-5.96	-5.76	-7.69	-6.99	-6.65	-6.22
	7	-6.99	-2.04	-0.955	-0.532	0.319	1.10	-10.53	-8.09	-7.54	-7.36	-6.93	-6.52	-5.76	-7.69	-6.99	-6.65	-6.22	-6.06
5	1	-0.217	1.31	1.73	1.91	2.14	2.01	-6.80	-6.05	-5.86	-5.78	-5.66	-5.61	-6.5	-5.61	-5.41	-5.36	-5.40	-5.19
	2	-1.29	0.302	1.35	1.74	1.82	1.90	-7.35	-6.52	-6.00	-5.84	-5.83	-5.69	-7.03	-6.19	-5.66	-5.53	-5.54	-5.37
	3	-2.33	-0.469	0.956	1.38	1.54	1.45	-7.81	-6.92	-6.17	-5.98	-5.90	-5.87	-7.54	-6.64	-5.91	-5.71	-5.63	-5.58
	4	-4.60	-1.39	0.085	1.21	1.16	1.41	-8.94	-7.35	-6.65	-6.10	-6.13	-5.93	-8.68	-7.09	-6.32	-5.84	-5.82	-5.57
	5	-6.09	-1.50	-0.196	1.04	1.32	1.56	-9.72	-7.42	-6.79	-6.20	-5.91	-5.87	-9.46	-7.15	-6.52	-5.93	-5.64	-5.59
	7	-6.06	-1.91	-0.825	0.424	1.00	1.19	-9.72	-7.63	-7.09	-6.51	-6.24	-6.06	-9.43	-7.27	-6.82	-6.17	-5.90	-5.78
6	1	-0.360	2.36	1.41	1.73	2.04	2.19	-5.55	-4.11	-4.71	-4.46	-4.36	-4.29	-5.08	-4.05	-4.13	-3.94	-3.85	-3.88
	2	0.088	1.53	2.07	2.68	3.10	2.91	-5.24	-4.44	-3.90	-3.90	-3.72	-3.88	-5.13	-4.31	-3.91	-3.81	-3.62	-3.81
	3	-2.89	-0.617	0.139	0.992	1.37	1.13	-6.57	-5.36	-5.12	-4.35	-4.46	-4.65	-6.04	-4.90	-4.63	-3.95	-4.02	-4.28
	4	-6.17	-1.13	-1.07	0.339	1.50	1.46	-8.19	-5.58	-5.68	-4.90	-4.38	-4.53	-7.75	-5.19	-5.25	-4.53	-4.33	-4.48
	5	-2.87	-0.422	0.162	0.938	1.05	1.27	-6.49	-5.18	-6.00	-4.55	-4.43	-3.85	-6.44	-5.14	-5.95	-4.51	-4.42	-3.81
	7	-5.13	-1.27	-0.709	0.555	-0.080	2.16	-7.59	-5.56	-5.40	-4.71	-5.07	-4.08	-7.52	-5.26	-5.05	-4.64	-4.77	-3.83
7	1	-8.12	-6.15	-5.72	-0.508	-3.98	-2.14	-7.75	-6.81	-6.59	-3.89	-5.83	-4.78	-7.53	-6.62	-6.43	-4.50	-5.74	-4.80
	2	-5.52	-3.20	-8.25	-2.56	-1.55	-0.665	-6.10	-5.07	-7.68	-4.77	-4.39	-4.02	-6.50	-5.55	-7.75	-5.17	-4.88	-4.53
	3	-8.71	-6.80	-6.31	-5.87	-4.98	-4.14	-7.65	-6.74	-6.53	-6.30	-6.01	-5.57	-7.57	-6.68	-6.49	-6.22	-5.99	-5.62
	4	-8.69	-6.80	-6.39	-5.75	-1.57	-4.78	-7.66	-6.72	-6.57	-6.23	-4.26	-5.99	-7.61	-6.72	-6.57	-6.20	-4.87	-5.99
	5	-5.02	-3.23	-2.92	-3.21	-1.89	-1.80	-5.74	-4.86	-4.77	-4.86	-4.37	-4.33	-6.38	-5.50	-5.40	-5.32	-4.99	-4.94
	7	-9.26	-7.22	-6.56	-6.29	-2.29	-5.14	-8.05	-7.03	-6.80	-6.64	-4.74	-6.19	-8.03	-7.02	-6.82	-6.59	-5.30	-6.26
8	1	-9.93	-8.22	-6.83	-6.41	-6.98	-5.40	-6.83	-5.94	-5.22	-5.18	-5.51	-4.70	-7.48	-6.60	-5.87	-5.89	-6.06	-5.49
	2	-6.92	-5.00	-3.63	-0.721	-3.01	-2.16	-5.22	-4.21	-3.71	-1.30	-3.12	-2.90	-6.48	-5.52	-5.10	-3.33	-4.54	-4.37
	3	-9.78	-8.99	-4.71	-6.52	-6.79	-6.69	-6.76	-5.76	-3.49	-5.10	-4.86	-4.93	-7.54	-6.57	-4.91	-5.93	-5.73	-5.73
	4	-11.3	-8.11	-9.64	-6.74	-6.84	-8.44	-6.97	-5.98	-6.03	-5.26	-5.02	-5.30	-7.72	-6.77	-6.72	-6.08	-5.72	-6.03
	5	-13.8	-10.1	-13.3	-5.42	-8.71	-3.03	-7.22	-6.22	-6.14	-3.77	-5.64	-3.43	-7.92	-6.96	-6.80	-5.11	-6.31	-4.79
	7	-6.99	-8.58	-8.31	-7.31	-7.40	-7.12	-5.79	-6.56	-6.41	-5.97	-5.97	-5.87	-7.04	-7.25	-7.06	-6.63	-6.59	-6.48
9	1	-10.4	-10.8	-9.25	-7.05	-7.00	-6.18	-2.94	-3.33	-2.51	-2.12	-1.58	-1.47	-6.73	-6.63	-5.90	-5.56	-5.11	-4.95
	2	-10.0	-9.58	-9.55	-10.8	-3.99	-6.73	-3.49	-2.19	-1.94	-1.87	-0.07	-0.92	-7.17	-5.99	-5.63	-5.49	-4.29	-4.69
	3	-14.6	-12.8	-12.5	-11.4	-11.6	-10.9	-3.56	-2.68	-2.66	-2.39	-2.18	-1.81	-7.23	-6.31	-6.13	-5.87	-5.64	-5.29
	4	-16.9	-16.0	-13.2	-14.6	-14.6	-14.6	-5.00	-4.60	-3.17	-3.96	-3.95	-3.94	-8.23	-7.63	-6.52	-6.96	-6.86	-6.76
	5	-18.0	-15.6	-14.3	-14.2	-14.1	-12.4	-5.61	-4.33	-3.67	-3.69	-3.63	-2.77	-8.66	-7.46	-6.87	-6.80	-6.67	-5.85
	7	-17.5	-15.5	-14.6	-12.5	-11.8	-13.2	-7.35	-6.41	-5.89	-4.90	-4.58	-5.18	-9.88	-8.90	-8.40	-7.64	-7.35	-7.65

References

[1] J. Popp, Z. Lakner, M. Harangi-Rákos, M. Fári, The effect of bioenergy expansion: Food, energy, and environment, Renewable and Sustainable Energy Reviews, 32 (2014) 559-578.
[2] M. Ahmad, A.U. Rajapaksha, J.E. Lim, M. Zhang, N. Bolan, D. Mohan, M. Vithanage, S.S. Lee, Y.S. Ok, Biochar as a sorbent for contaminant management in soil and water: a review, Chemosphere, 99 (2014) 19-33.
[3] S. Kumar, V.A. Loganathan, R.B. Gupta, M.O. Barnett, An Assessment of U(VI) removal from groundwater using biochar produced from hydrothermal carbonization, Journal of environmental management, 92 (2011) 2504-2512.
[4] J.M. Novak, I.X. Lima, Baoshan; , J.W. Gaskin, C. Steiner, K.C. Das, M. Ahmedna, D. Rehrah, D.W. Watts, W.J. Busscher, H. and Schomberg, Characterization of designer biochar produced at different temperatures and their effects on a loamy sand, Annals of Environmental Science, 3 (2009) 195-206.
[5] Z. Liu, F.-S. Zhang, J. Wu, Characterization and application of chars produced from pinewood pyrolysis and hydrothermal treatment, Fuel, 89 (2010) 510-514.
[6] C. Wang, M.T. Walter, J.Y. Parlange, Modeling simple experiments of biochar erosion from soil, Journal of Hydrology, 499 (2013) 140-145.
[7] J.H. Park, G.K. Choppala, N.S. Bolan, J.W. Chung, T. Chuasavathi, Biochar reduces the bioavailability and phytotoxicity of heavy metals, Plant and Soil, 348 (2011) 439-451.
[8] Z. Liu, F.S. Zhang, Removal of lead from water using biochars prepared from hydrothermal liquefaction of biomass, Journal of Hazardous Materials, 167 (2009) 933-939.
[9] M. Uchimiya, I.M. Lima, K. Thomas Klasson, S. Chang, L.H. Wartelle, J.E. Rodgers, Immobilization of heavy metal ions (CuII, CdII, NiII, and PbII) by broiler litter-derived biochars in water and soil, Journal of agricultural and food chemistry, 58 (2010) 5538-5544.
[10] M. Inyang, B. Gao, Y. Yao, Y. Xue, A.R. Zimmerman, P. Pullammanappallil, X. Cao, Removal of heavy metals from aqueous solution by biochars derived from anaerobically digested biomass, Bioresource technology, 110 (2012) 50-56.
[11] N. Borchard, K. Prost, T. Kautz, A. Moeller, J. Siemens, Sorption of copper (II) and sulphate to different biochars before and after composting with farmyard manure, European Journal of Soil Science, 63 (2012) 399-409.
[12] F. Rees, M.O. Simonnot, J.L. Morel, Short-term effects of biochar on soil heavy metal mobility are controlled by intra-particle diffusion and soil pH increase, European Journal of Soil Science, 65 (2014) 149-161.
[13] Z.-b. Zhang, X.-h. Cao, P. Liang, Y.-h. Liu, Adsorption of uranium from aqueous solution using biochar produced by hydrothermal carbonization, Journal of Radioanalytical and Nuclear Chemistry, 295 (2012) 1201-1208.
[14] L. Field, T. Barnie, J. Blundy, R.A. Brooker, D. Keir, E. Lewi, K. Saunders, Integrated field, satellite and petrological observations of the November 2010 eruption of Erta Ale, Bulletin of Volcanology, 74 (2012) 2251-2271.
[15] N.J. Nnaji, J.U. Ani, A.M. and Ekwonu, The solution of reversible first order reaction equation revisited, Acta Chimica & Pharmaceutica Indica, 3 (2013) 212-218.
[16] L.M. Brown, H.S. Sherry, F.J. Krambeck, Mechanism and kinetics of isotopic exchange in zeolites. I. Theory, The Journal of Physical Chemistry, 75 (1971) 3846-3855.
[17] W.H. Shetaya, S.D. Young, M.J. Watts, E.L. Ander, E.H. Bailey, Iodine dynamics in soils, Geochimica et Cosmochimica Acta, 77 (2012) 457-473.
[18] Z. Rong, P. Vadgama, Simple expressions for diffusion coefficient determination of adsorption within spherical and cylindrical absorbents using direct simulation method, Journal of colloid and interface science, 303 (2006) 75-79.

[19] J.B. Cliff, P.J. Bottomley, R. Haggerty, D.D. and Myrold, Modeling the effects of diffusion limitations on nitrogen-15 isotope dilution experiments with soil aggregates, Soil Science Society of America Journal, 66 (2002) 1868–1877.
[20] S. Altfelder, T. Streck, Capability and limitations of first-order and diffusion approaches to describe long-term sorption of chlortoluron in soil, Journal of contaminant hydrology, 86 (2006) 279-298.
[21] I.R. Iznaga, V. Petranovskii, G.R. Fuentes, C. Mendoza, A.B. Aguilar, Exchange and reduction of Cu^{2+} ions in clinoptilolite, Journal of Clloid and Interface Science, 316 (2007) 877-886.
[22] E. Costa, G. Calleja, F. Domingo, Adsorption of gaseous hydrocarbons on activated carbon: Characteristic kinetic curve, AIChE Journal, 31 (1985) 982-991.
[23] A. Mittal, L. Kurup, V.K. Gupta, Use of waste materials—Bottom Ash and De-Oiled Soya, as potential adsorbents for the removal of Amaranth from aqueous solutions, Journal of Hazardous Materials, 117 (2005) 171-178.
[24] E.R. Marzouk, S.R. Chenery, S.D. Young, Measuring reactive metal in soil: a comparison of multi-element isotopic dilution and chemical extraction, European Journal of Soil Science, 64 (2013) 526-536.
[25] Z.-Y. Huang, T. Chen, J. Yu, X.-C. Zeng, Y.-F. Huang, Labile Cd and Pb in vegetable-growing soils estimated with isotope dilution and chemical extractants, Geoderma, 160 (2011) 400-407.
[26] R.E. Hamon, D.R. Parker, E. Lombi, Advances in Isotopic Dilution Techniques in Trace Element Research: A Review of Methodologies, Benefits, and Limitations, in: Isotopic Dilution Book Advances in Agronomy (Advances in Agronomy), 2008.
[27] I.A.M. Ahmed, N.M.J. Crout, S.D. Young, Kinetics of Cd sorption, desorption and fixation by calcite: A long-term radiotracer study, Geochimica et Cosmochimica Acta, 72 (2008) 1498-1512.
[28] R. Han, W. Zou, Y. Wang, L. Zhu, Removal of uranium(VI) from aqueous solutions by manganese oxide coated zeolite: discussion of adsorption isotherms and pH effect, Journal of environmental radioactivity, 93 (2007) 127-143.
[29] X. Shuibo, Z. Chun, Z. Xinghuo, Y. Jing, Z. Xiaojian, W. Jingsong, Removal of uranium (VI) from aqueous solution by adsorption of hematite, Journal of environmental radioactivity, 100 (2009) 162-166.
[30] G. Wang, J. Liu, X. Wang, Z. Xie, N. Deng, Adsorption of uranium (VI) from aqueous solution onto cross-linked chitosan, Journal of Hazardous Materials, 168 (2009) 1053-1058.
[31] S. Lofts, E. Tipping, Assessing WHAM/Model VII against field measurements of free metal ion concentrations: model performance and the role of uncertainty in parameters and inputs, Environmental Chemistry, 8 (2011) 501-516.
[32] J.S. Arey, J.C. Seaman, P.M. Bertsch, Immobilization of Uranium in Contaminated Sediments by Hydroxyapatite Addition, Environmental science & technology, 33 (1999) 337-342.
[33] B. Ozkaya, Adsorption and desorption of phenol on activated carbon and a comparison of isotherm models., Journal of Hazardous Materials, 129 (2006) 158-163.
[34] M.J. Beazley, R.J. Martinez, P.A. Sobecky, S.M. Webb, M. Taillefert, Uranium Biomineralization as a Result of Bacterial Phosphatase Activity: Insights from Bacterial Isolates from a Contaminated Subsurface, Environmental Science and Technology, 41 (2007) 5701-5707.
[35] C.C. Fuller, J.R. Bargar, J.A. Davis, M.J. Piana, Mechanisms of uranium interaction with hydroxyapatite: Implications for groundwater remediation, Environmental Science & Technology, 36 (2002) 158-165.
[36] A. Singh, J.G. Catalano, U. Kai-Uwe, D.E. Giammar, Molecular-scale structure of uranium(VI) immobilized with goethite and phosphate, Environmental Science & Technology, 46 (2012) 6594-6603.
[37] J. Jeanjean, J.C. Rouchaud, L.a. Tran, M. Fedoroff, Sorption of uranium and other heavy metals on hydroxyapatite, Journal of Radioanalytical and Nuclear Chemistry Letters, 201 (1995) 529-539.

[38] V.S. Mehta, F. Maillot, Z. Wang, J.G. Catalano, D.E. Giammar, Effect of reaction pathway on the extent and mechanism of uranium(VI) immobilization with calcium and phosphate. , Environmental Science & Technology, 50 (2016) 3128-3136.
[39] J.Y. Lee, J.I. Yun, Formation of ternary $CaUO_2(CO_3)_3^{2-}$ and $Ca_2UO_2(CO_3)_3(aq)$ complexes under neutral to weakly alkaline conditions, Dalton Transactions, 42 (2013) 9862-9869.
[40] J.R. Bargar, R. Reitmeyer, J.J. Lenhart, J.A. Davis, Characterization of U(VI)-carbonato ternary complexes on hematite: EXAFS and electrophoretic mobility measurements, Geochimica et Cosmochimica Acta, 64 (2000) 2737-2749.
[41] D. Gorman-Lewis, P.C. Burns, J.B. Fein, Review of uranyl mineral solubility measurements, The Journal of Chemical Thermodynamics, 40 (2008) 335-352.
[42] D. Gorman-Lewis, J.B. Fein, P.C. Burns, J.E.S. Szymanowski, J. Converse, Solubility measurements of the uranyl oxide hydrate phases metaschoepite, compreignacite, Na–compreignacite, becquerelite, and clarkeite, The Journal of Chemical Thermodynamics, 40 (2008) 980-990.
[43] D. Gorman - lewis, T. Shvareva, K.-A. Kubatko , P.C. Burns , D.M. Wellman , B. Mcnamara , J.S. Szymanowski , A. Navrotsky , J.B. and Fein, Thermodynamic Properties of Autunite, Uranyl Hydrogen Phosphate, and Uranyl Orthophosphate from Solubility and Calorimetric Measurements, Environmental science & technology, 43 (2009) 7416–7422.